CML 89-2

Orthotropic Elasto-Plastic Behavior of AS4/APC-2 Thermoplastic Composite in Compression

by

C. T. Sun and Y. Rui

NAG1-825

April 1989

A Technical Report Prepared for
NASA Langley Research Center
Hampton, Virginia

This research was supported by NASA
Langley Research Center under Grant No. NAG-1-825.

Abstract

Uniaxial compression tests were performed on off-axis coupon specimens of unidirectional AS4/APC-2 thermoplastic composite at various temperatures. The elasto-plastic and strength properties of AS4/APC-2 composite were characterized with respect to temperature variation by using a one-parameter orthotropic plasticity model and a one-parameter failure criterion. Experimental results showed that the orthotropic plastic behavior can be characterized quite well using the plasticity model, and the matrix-dominant compressive strengths can be predicted very accurately by the one-parameter failure criterion.

1. Introduction

AS4/APC-2 is a high-performance thermoplastic composite material consisting of thermoplastic matrix PEEK (polyether ether ketone) reinforced with continuous AS4 graphite fibers. Compared with other types of thermoplastic matrix, PEEK has higher ductility, higher operating temperature and is unaffected by solvents. Due to the higher ductility of the matrix, AS4/APC-2 exhibits greater plasticity.

A number of models have been developed to describe the nonlinear stress-strain relations in many fiber composites. Hahn and Tsai (1973) employed a complementary elastic energy density function which contains a biquadratic term for in-plane shear stress. As a result, the stress-strain relation is linear in simple longitudinal and transverse extensions. Dvorak and Bahei-El-Din (1979, 1982) used a micromechanical model consisting of elastic filaments of vanishing diameters and an elastic-plastic matrix. As noted by Bahei-El-Din and Dvorak (1980), the difficulties encountered in formulating micromodels lie in the facts that constituent matrix properties in-situ are different from those of bulk matrix material and that 3-D elastic constants of the fiber are difficult to measure. Recently, Johnson et al (1988) indicated that the fiber-matrix interfacial bond in some metal-matrix composites is very weak as opposed to the perfect bond assumed in developing these micromechanical models.

For unidirectional composites, their plastic behavior can be considered orthotropic. Kenaga et al (1987) proposed a three parameter plasticity model to characterize the nonlinear behavior of unidirectional composites. Since most fiber composites exhibit insignificant plasticity in the longitudinal direction, and the plastic deformation of composites is dominated by matrix plasticity, Sun and Chen (1987) further proposed a one-parameter plasticity model, in which the parameter can be obtained from simple uniaxial tension tests of off-axis specimens. Sun and Yoon (1988) used this model to describe the nonlinear stress-strain relations for AS4/APC-2

composite in tension with excellent result. This model, because of its simple testing procedure, is especially attractive for characterizing plastic properties of unidirectional composites in elevated temperature environments.

The present study aims at characterizing the compressive elasto-plastic and strength properties of AS4/APC-2 composite with respect to temperature variation using the one parameter plasticity model and a one-parameter failure criterion.

2. Experimental Procedure

Specimens and Tabs

The 0°, 5°, 15°, 30°, 45°, and 90° coupon specimens were cut from $[0_{10}]$ panels. The thickness was 1.27 ± 0.03 mm. The specimen length was 229 mm and the width was 25.4 mm.

Applying uniaxial stress on off-axis composite specimens is a challenge due to the extension-shear coupling in these specimens (Pagano and Halpin, 1968). If rigid grips are used, a nonuniform stress field would be produced. To achieve a uniform stress field, one can use either a long specimen or flexible end tabs developed by Sun and Berreth (1988).

In this study, two kinds of flexible tabs were used for off-axis compression tests of AS4/APC-2. The flexible tab made of Flex Epoxy 103 and fiber-glass knit was used for tests at room temperature. The flexible tab made of FM1000 adhesive film and fiber-glass knit was used for tests at 250° F. Aluminum tabs were used for tests at 150° F.

Anti-buckling Apparatus

An anti-buckling apparatus was designed and used in the compression test. This apparatus shown in Fig. 1 has the following functions:

- It allows the specimen to have a long effective specimen length in order to reduce the end effect due to compression-shear coupling.
- The plane stress state of the specimen should not be affected. In other words, lateral pressure on the specimen should be kept low.

This anti-buckling apparatus was designed for compression tests on off-axis coupon specimens. The effective specimen length was 152 mm. The specimen was supported by four steel guides. The lateral supporting force was exerted using six springs resulting in 890 N of supporting force. The corresponding normal stress due to the supporting force is about 0.23 MPa.

In order to reduce the surface friction between the specimen and the steel guides, a TX-1040 teflon-coated fabric sheet was put between the specimen and the steel guide. The maximum friction force between the specimen and the steel guide can be reduced to 195 N. The stresses caused by the friction force is neglectable.

Test Procedures

Uniaxial compression tests were performed using the closed-loop-servo-hydraulic MTS 810 machine at 75°F, 150°F and 250°F. The specimen was heated and tested in a heating chamber (Model F–2–CH–CO_2 , Thermotron Corp.).

All tests were performed at a strain-controlled mode at the strain rate of $5x10^{-6}$ m/m/s. Longitudinal and transverse strains were measured by strain gages mounted at the center of the specimen. The measured analog signals were converted into digital signals which were stored and analyzed by an IBM-AT computer data acquisition system.

3. Experimental Results and Discussion

The stress-strain curves for the 0°, 15°, 30°, 45° and 90° coupon specimens tested at 75°F, 150°F and 250°F are shown in Figs. 2-4.

Modulus

The apparent compressive moduli of the off-axis coupon specimens are listed in Table 1. As expected the longitudinal modulus hardly changes with respect to temperature variation. The apparent moduli at 250°F of off-axis specimens drop to 85-90% of the room temperature moduli. Since the longitudinal modulus is dominated by the graphite fibers, and the off-axis moduli are dominated by the APC-2 matrix, it can be concluded that the modulus of fibers is not sensitive to temperature variation, but the modulus of matrix is sensitive to temperature variation.

Failure Modes and Strengths

Failure of the 0° coupon specimen was accompanied by a brush-like failure surface. For the 5° and 15° specimens, where fiber micro-buckling was observed, there were two failure surfaces: one, parallel to the fiber direction; the other, caused by the micro-buckling, making an angle of 80° with the fiber. The failure surfaces of 20°, 30° and 45° specimens were parallel to the fibers. The failure surface of 90° specimen was parallel to the fibers but inclined at 45° across the thickness of the specimen.

The apparent compressive strengths of the off-axis coupon specimens are summerized in Table 1, which shows that the apparent compressive strength decreases as temperature increases. It is interesting to note that both longitudinal and off-axis compressive strengths are sensitive to temperature variation. This implies that the matrix stiffness property can affect the longitudinal compressive strength of a fiber composite. Sun and Yoon (1988) found that the tensile strength of AS4/APC-2 composite is insensitive to temperature variation up to 350°F.

4. One Parameter Plasticity Model

According to the one-parameter plasticity model (Sun and Chen, 1987), a plastic potential is defined by

$$2f = \sigma_{22}^2 + 2a_{66}\sigma_{12}^2 \tag{1}$$

where a_{66} is the material parameter, σ_{22} and σ_{12} are stresses referring to the material principal axes x_1 and s_2 with the x_1−axis in the fiber direction. From the plastic potential, the plastic strain increments are derived:

$$\begin{Bmatrix} d\varepsilon_{11}^p \\ d\varepsilon_{22}^p \\ d\gamma_{12}^p \end{Bmatrix} = \begin{Bmatrix} \dfrac{\partial f}{\partial \sigma_{11}} \\ \dfrac{\partial f}{\partial \sigma_{22}} \\ \dfrac{\partial f}{\partial \sigma_{12}} \end{Bmatrix} = \begin{Bmatrix} 0 \\ \sigma_{22} \\ 2a_{66}\sigma_{12} \end{Bmatrix} d\lambda \tag{2}$$

where γ_{12} is the in-plane engineering shear strain.

The corresponding effective stress and effective plastic strain increments are defined by

$$\bar{\sigma} = \left[\frac{3}{2}(\sigma_{22}^2 + 2a_{66}\sigma_{12}^2)\right]^{\frac{1}{2}} \tag{3}$$

and

$$d\bar{\varepsilon}^p = \left[\frac{2}{3}(\sigma_{22}^2 + 2a_{66}\sigma_{12}^2)\right]^{\frac{1}{2}} d\lambda \tag{4}$$

respectively. The complete orthotropic plastic flow rule is defined as the parameters a_{66} and $d\lambda$ are determined.

Off-Axis Compression Test

The material parameter a_{66} and the relation of effective stress versus effective strain were determined from static compression tests on off-axis coupon specimens.

Let x-axis be the uniaxial loading direction which makes an angle θ with the fiber direction along the x_1-axis. The stresses referring to the material principal axes (x_1 and x_2) are related to the applied uniaxial stress σ_x as

$$\begin{aligned} \sigma_{11} &= \cos^2\theta\ \sigma_x \\ \sigma_{22} &= \sin^2\theta\ \sigma_x \\ \sigma_{12} &= -\sin\theta\cos\theta\ \sigma_x \end{aligned} \tag{5}$$

Substitution of (5) into (3) yields

$$\bar{\sigma} = h(\theta)\ \sigma_x \tag{6}$$

where

$$h(\theta) = \sqrt{\frac{3}{2}} \left[\sin^4\theta + 2a_{66}\sin^2\theta\cos^2\theta\right]^{\frac{1}{2}} \tag{7}$$

Using a similar coordinate transformation for strains and the definition for $d\bar{\varepsilon}^p$ as given by (4), we obtain

$$d\bar{\varepsilon}^p = d\varepsilon_x^p / h(\theta) \tag{8}$$

where $d\varepsilon_x^p$ is the plastic strain increment in the x-direction. Thus, the desired relation between $\bar{\sigma}$ and $\bar{\varepsilon}^p$ can now be derived from the experimentally obtained relation between σ_x and ε_x^p. It follows that

$$\frac{d\bar{\sigma}}{d\bar{\varepsilon}^p} = h^2(\theta)\,\frac{d\sigma_x}{d\varepsilon_x^p} \tag{9}$$

and

$$d\lambda = \frac{3}{2}\,\frac{1}{h^2(\theta)}\,\frac{d\varepsilon_x^p}{d\sigma_x}\,\frac{d\sigma_x}{\sigma_x} \tag{10}$$

For different values of θ , the resulting $\bar{\sigma}/\bar{\varepsilon}^p$ curves must be identical. This is achieved by selecting a proper value for a_{66}.

Experimental results indicate that for fiber composites there is no well defined yield point. In view of this, the master effective stress-effective plastic strain curve can be fitted by a power law, as

$$\bar{\varepsilon}^p = A(\bar{\sigma})^n \tag{11}$$

Parameter and Coefficient Evaluation

The effective stress-effective plastic strain relations of all off-axis specimens at 75°F, 150°F and 250°F are shown in Figs. 5-7, respectively. It was reported in Sun and Yoon (1988) that a_{66}=1.5 is suitable for AS4/APC-2 thermoplastic composite in tension within the temperature range from 75°F to 350°F. In the present study, it was found that a_{66}=1.7 is suitable for compression. This implies that in compression the normal stress σ_{22} has less contribution to plasticity in the composite than the shear stress σ_{12}.

The effective stress-effective plastic strain data of each off-axis angle are collapsed into one curve with a_{66}=1.7 for all temperatures. This indicates that the plastic orthotropy of AS4/APC-2 composite is independent of temperature within this temperature range.

By taking the logarithm of (11) and fitting it with the experimental data, we can obtain coefficients A and n which are summarized in Table 2. Parameter n = 5.0 is adequate for temperatures up to 250°F, and coefficient A is related to temperature as

$$\ln(A) = 0.0089T - 31.6 \tag{12}$$

The value of ln(A) versus temperature is plotted in Fig. 8. Note that in using (11) and (12) T must be in °F and $\bar{\sigma}$ in MPa.

By adding the elastic strain component to the plastic component, the total strain in the off-axis specimen is obtained as

$$\varepsilon_x = \frac{\sigma_x}{E_x} + \varepsilon_x^p = \frac{\sigma_x}{E_x} + \left[h(\theta)\right]^{n+1} A\sigma_x^n \tag{13}$$

where E_x is the apparent elastic modulus.

Figures 9-11 show the experimental and predicted total stress-strain curves for the off-axis specimens at each testing temperature. Agreement between experimental data and prediction is excellent.

Plastic Poisson's Ratio

The plastic Poisson's ratio is defined as

$$\nu_\theta^p = -\frac{d\varepsilon_y^p}{d\varepsilon_x^p} \tag{14}$$

From (2) and the transformation law on strain components, the plastic strain increments in x and y directions can be obtained. Using these expressions and (14), we obtain

$$\nu_\theta^p = \frac{(2a_{66}-1)\cos^2\theta}{\sin^2\theta + 2a_{66}\cos^2\theta} \tag{15}$$

Thus, according to the one-parameter plasticity model, the plastic Poisson's ratio only depends on the fiber orientation but not the strain level. Using the longitudinal and transverse stress-strain curves of the off-axis specimens with a strain increment $d\varepsilon_x = 0.0008$, the plastic strain increments $d\varepsilon_x^p$ and $d\varepsilon_y^p$ were calculated, with which the plastic Poisson's ratio was obtained from (14). In general, the plastic Poisson's ratio obtained in the manner depends on the strain level. Figure 12 shows the average plastic Poisson's ratios measured from the experimental stress-strain curves and the predicted values. For $\theta = 15^\circ$ and 45°, the predicted plastic Poisson's ratios agree with the experimental values very well. For $\theta = 30^\circ$, some discrepancy is noted.

5. One Parameter Failure Criterion

For matrix-dominant failure, the one parameter failure criterion is given by

$$\sigma_{22}^2 + 2a_{66}^* \sigma_{12}^2 = k_{cr}^2 \tag{16}$$

where k_{cr} is a critical value and a_{66}^* a strength orthotropy parameter to be determined.

Fiber breakage is an alternate mode of failure for small angle off-axis specimens. The failure criterion for fiber breakage is assumed to be

$$\sigma_{11} \leq X' \tag{17}$$

where X' is the longitudinal compressive strength.

From (16), the following relations can be derived:

$$k_{cr} = Y' \ , \quad 2a_{66}^* = \frac{Y'^2}{S^2} \tag{18}$$

where Y' is the transverse compressive strength. Thus, criterion (16) can be determined by measuring Y' and S independently. Alternatively, the values of k_{cr} and a_{66}^* can be determined from the off-axis test results. In the latter case, the in-plane shear strength S can be obtained from (18).

Experimental value of the parameters a_{66}^* and k_{cr}^2 are summarized in Table 3. It can be seen that a_{66}^* is not sensitive to temperature variation, but k_{cr} decreases as temperature increases. Through linear curve fitting, we obtained

$$k_{cr}^2 = -71.2T + 3.66 \times 10^4 \tag{19}$$

where T is in ^{o}F and k_{cr} in MPa. The parameter k_{cr}^2 versus temperatures is plotted in Fig. 13.

The experimental data and the predicted strengths from the one parameter criterion and Tsai-Hill criterion (Jones, 1975) are compared in Figs. 14-16. The values of X′ and Y′ used in the Tsai-Hill criterion are X′ = 1234 MPa (75°F), 1036 MPa (150°F), 985 MPa (250°F), and Y′ = 176 MPa (75°F), 163 MPa (150°F), 136 MPa (250°F). The two criteria agree very well except for small off-axis angles. To compare the Tsai-Hill failure criterion and the one parameter failure criterion in the small off-axis angle region, the 5° off-axis specimen was tested at room temperature. The experimental result and predictions by Tsai-Hill criterion and the one-parameter model are 728 MPa, 768 MPa and 954 MPa, respectively. The prediction by Tsai-Hill criterion is closer to the experimental data.

The in-plane shear strength can be obtained from the apparent strengths of off-axis specimens using either the Tsai-Hill failure criterion or the one parameter failure criterion. In the Tsai-Hill failure criterion, the shear strength is given by

$$S = \left[\frac{\cos^2\theta \sin^2\theta}{\frac{1}{\sigma_{ult}^2} - \left[\frac{\cos^2\theta}{X'}\right]^2 - \left[\frac{\sin^2\theta}{Y'}\right]^2 + \left[\frac{\sin^2\theta}{X'}\right]\left[\frac{\cos^2\theta}{X'}\right]} \right]^{\frac{1}{2}} \tag{20}$$

where σ_{ult} is the apparent strength of the off-axis specimen with angle θ.

In the one parameter failure criterion shear strength can be expressed as

$$S = \left[\frac{Y'^2}{2a_{66}^*} \right]^{\frac{1}{2}} \tag{21}$$

Table 4 shows that the shear strengths calculated from (20) and (21) are almost the same. However, some variation with respect to the loading angle is noted in the one-parameter failure model.

6. Conclusion

Compressive elasto-plastic behavior of AS4/APC-2 thermoplastic composite can be well characterized by using the one-parameter plasticity model. As material parameters, the orthotropic plasticity parameter a_{66} and the power index n are not affected by temperature variation, and the logarithm of coefficient A varies linearly with temperature within the temperature range from 75°F to 250°F.

The compressive failure strengths of off-axis specimens can be predicted by using the one parameter failure criterion. As a material parameter, the strength orthotropy parameter a^*_{66} is not sensitive to temperature variation. The critical value k^2_{cr} is a linear function of temperature.

The stress-strain relations in compression are different from those in tension. Thus, the parameters a_{66}, A, n, a^*_{66} and k_{cr} in compression and tension are different.

Acknowledgment

This research was sponsored by NASA Langley Research Center under Grant No. NAG-1-825 with Dr. Catherine A. Bigelow as technical monitor.

7. References

Bahei-El-Din, Y.A. and Dvorak, G.J. (1980), "Plastic deformation of a laminated plate with a hole", *J. Appl. Mech., 47,* 827.

Dvorak, G.J. and Bahei-El-Din, Y.A. (1979), "Elastic-plastic behavior of fibrous composites", *J. Mech. Phys. Solids, 27,* 51.

Dvorak, G.J. and Bahei-El-Din, Y.A. (1982), "Plasticity analysis of fibrous composites", *J. Appl. Mech., 49,* 327.

Hahn, H.T. and Tsai, S.W. (1973), "Nonlinear elastic behavior of unidirectional composite laminates", *J. Composite Mat., 7,* 102.

Johnson, W.S., Lubowinski, S.J., Highsmith, A.L., Brewer, W.D. and Hoogstraten, C.A. (1988), "Mechanical characterization of SCS6/Ti-15-3 metal matrix composites at room temperature", *NASP Technical Memorandum 1014,* NASA-Langley Research Center, Hampton, Virginia.

Jones, R.M. (1975), *Mechanics of Composite Materials,* Scripta Book Company, Washington, D.C.

Kenaga, D., Doyle, J.F. and Sun, C.T. (1987), "The characterization of boron/aluminum composite in the nonlinear range as an orthotropic elastic-plastic material", *J. Composite Mat., 21,* 516.

Pagano, N.J. and Halpin, J.C. (1968), "Influence of end constraints in the testing of anisotropic bodies", *J. Composite Mat., 2,* 18.

Sun, C.T. and Berreth, S. (1988), "A new tab design for off-axis tension test", *J. Composite Mat., 22,* 766.

Sun, C.T. and Chen, J.L. (1987), "A simple flow rule for characterizing nonlinear behavior of fiber composites", *J. Composite Mat., 23,* 1009.

Sun, C.T. and Yoon, K.J. (1988), "Characterization of elastic-plastic properties of AS4/APC-2 thermoplastic composite", to be published.

Table 1. Apparent compressive elastic moduli and strengths of different off-axis specimens at various temperatures.

Angle (degree)	Temp. (°F)	Modulus (GPa)	Strength (MPa)	Poisson's Ratio
0°	75	130.8	1234	0.33
	150	129.2	1036	0.33
	250	129.9	985	0.34
15°	75	62.6	310	0.37
	150	57.3	277	0.39
	250	57.2	240	0.38
30°	75	25.1	192	0.36
	150	23.9	172	0.34
	250	22.5	152	0.39
45°	75	16.9	152	0.25
	150	16.7	145	0.27
	250	13.9	121	0.24
90°	75	10.7	176	0.012
	150	10.3	163	0.013
	250	9.7	136	0.012

Table 2. Variations of coefficients A and n with temperature for a_{66}=1.7.

Coeff.	75°F	150°F	250°F
n	5.0	5.0	5.0
A (MPa^{-5})	$4.0x10^{-14}$	$6.8x10^{-14}$	$1.9x10^{-13}$

Table 3. Variations of a_{66}^{*} and k_{cr} with temperature.

Angle	75°F		150°F		250°F	
	a_{66}^{*}	k_{cr} (MPa)	a_{66}^{*}	k_{cr} (MPa)	a_{66}^{*}	k_{cr} (MPa)
15°	2.54		2.73		2.53	
30°	2.06		2.22		1.97	
45°	2.16		2.02		2.03	
Average	2.25	176	2.32	163	2.18	136

Table 4. Shear strengths (MPa) at various temperatures obtained from Tsai-Hill failure criterion and one-parameter failure criterion.

Angle	75°F		150°F		250°F	
	Tsai-Hill	One-Parameter	Tsai-Hill	One-Parameter	Tsai-Hill	One-Parameter
15°	81.3	77.9	72.3	69.6	62.0	60.6
30°	87.5	86.8	77.9	77.2	68.9	68.2
45°	84.7	84.7	80.6	80.6	67.5	67.5
Average	84.7	83.4	77.2	75.8	66.1	65.5

Figure Captions

Fig. 1. Schematic of anti-buckling apparatus for compression test of off-axis coupon specimens (unit: mm).

Fig. 2. Compressive stress-strain curves for off-axis specimens of AS4/APC-2 at 75°F.

Fig. 3. Compressive stress-strain curves for off-axis specimens of AS4/APC-2 at 150°F.

Fig. 4. Compressive stress-strain curves for off-axis specimens of AS4/APC-2 at 250°F.

Fig. 5. Effective stress-effective strain curves for off-axis specimens of AS4/APC-2 with $a_{66} = 1.7$ at 75°F.

Fig. 6. Effective stress-effective strain curves for off-axis specimens of AS4/APC-2 with $a_{66} = 1.7$ at 150°F.

Fig. 7. Effective stress-effective strain curves for off-axis specimens of AS4/APC-2 with $a_{66} = 1.7$ at 250°F.

Fig. 8. Variation of ln(A) with temperature (unit of A: MPa sup -5).

Fig. 9. Comparison of compressive stress-strain curves for off-axis specimens of AS4/APC-2 obtained from experiment and from the one-parameter plasticity model at 75°F.

Fig. 10. Comparison of compressive stress-strain curves for off-axis specimens of AS4/APC-2 obtained from experiment and from the one-parameter plasticity model at 150°F.

Fig. 11. Comparison of compressive stress-strain curves for off-axis specimens of AS4/APC-2 obtained from experiment and from the one-parameter plasticity model at 250°F.

Fig. 12. Plastic Poisson's ratios jof AS4/APC-2 obtained from experiment and from the one-parameter plasticity model with $a_{66} = 1.7$.

Fig. 13. Variation of k_{cr}^2 with temperature.

Fig. 14. Comparison of compressive strengths for off-axis specimens of AS4/APC-2 obtained from experiment, Tsai-Hill criterion and one-parameter criterion at 75°F.

Fig. 15. Comparison of compressive strengths for off-axis specimens of AS4/APC-2 obtained from experiment, Tsai-Hill criterion and one-parameter criterion at 150°F.

Fig. 16. Comparison of compressive strengths for off-axis specimens of AS4/APC-2 obtained from experiment, Tsai-Hill criterion and one-parameter criterion at 250°F.

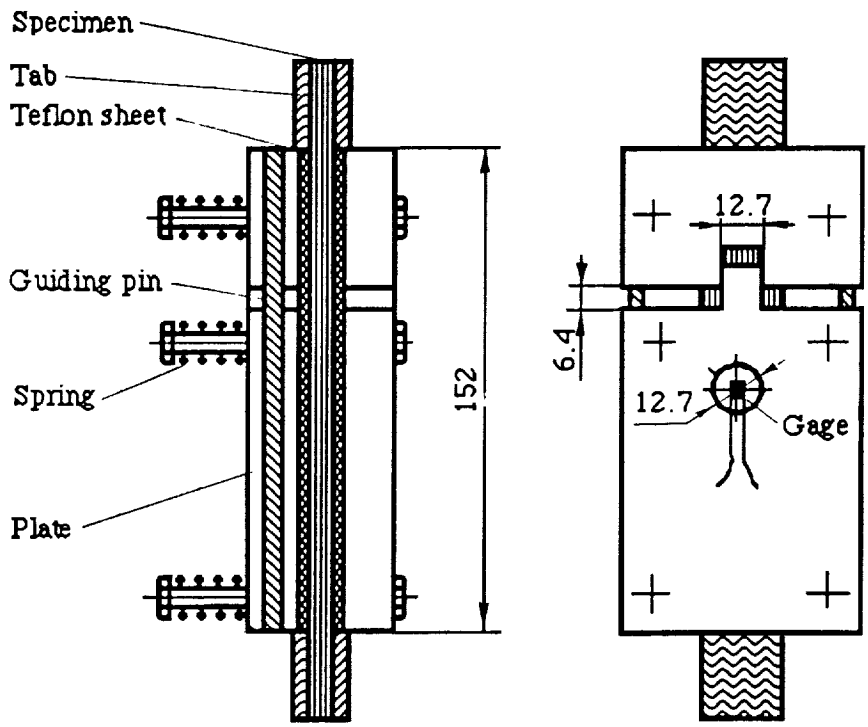

Fig. 1. Schematic of anti-buckling apparatus for compression test of off-axis coupon specimens (unit: mm).

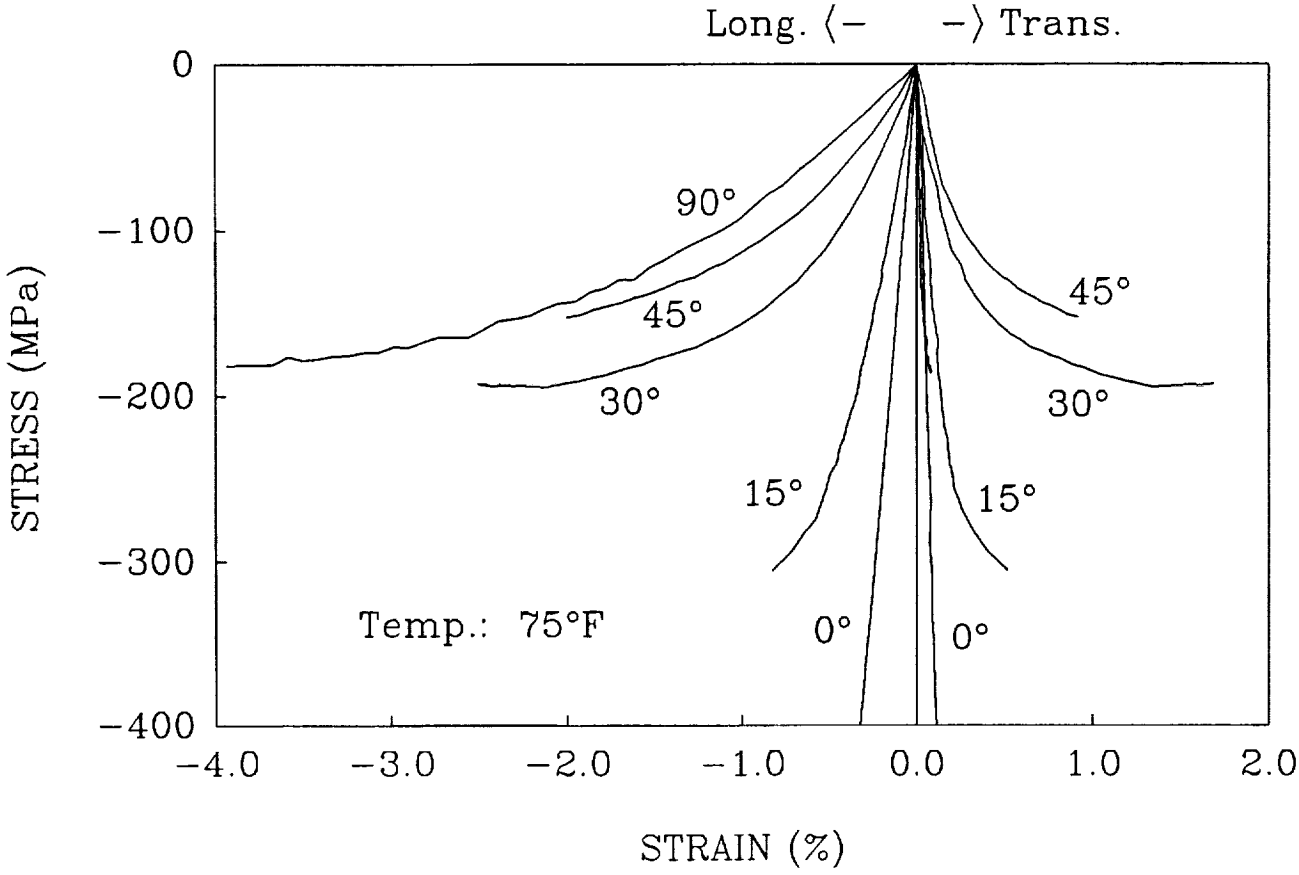

Fig. 2. Compressive stress-strain curves for off-axis specimens of AS4/APC-2 at 75°F.

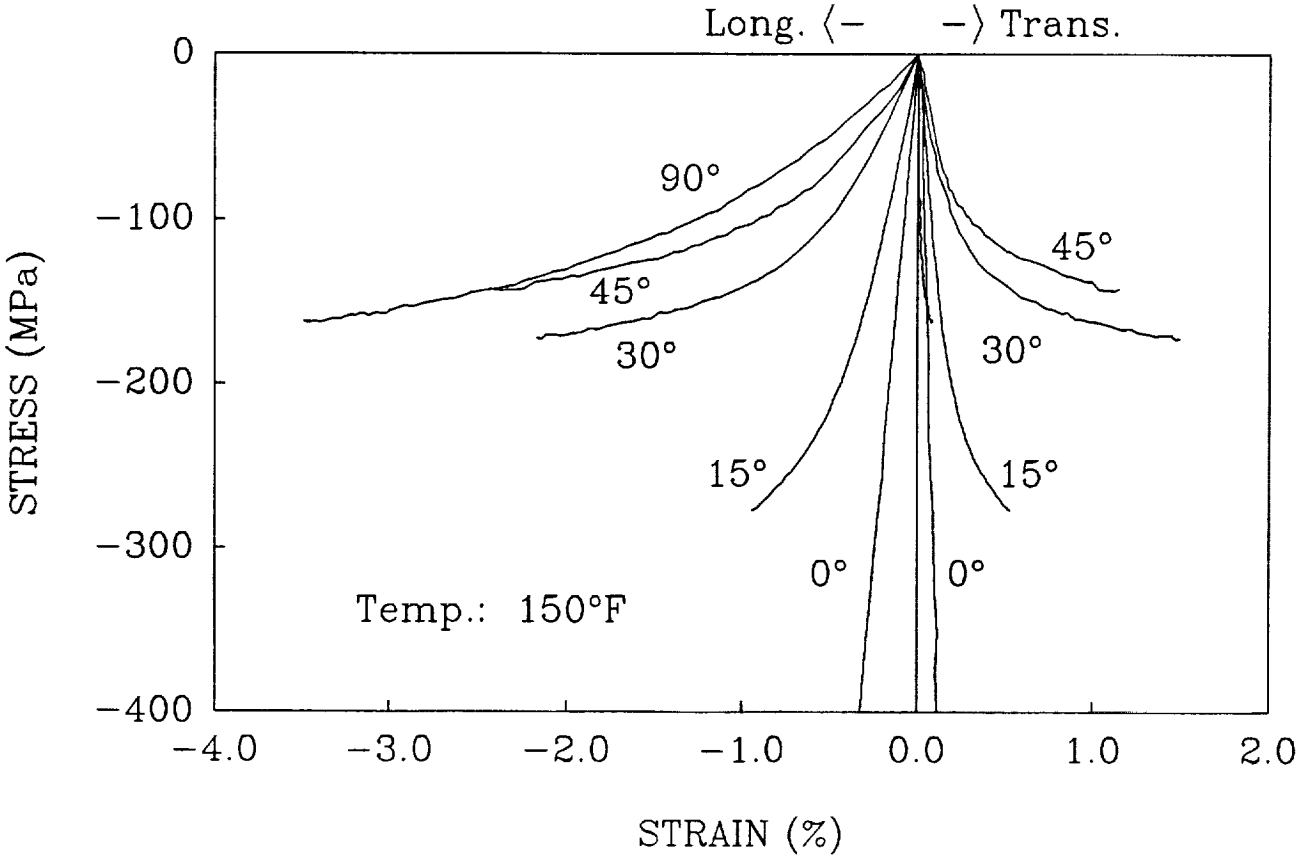

Fig. 3. Compressive stress-strain curves for off-axis specimens of AS4/APC-2 at 150°F.

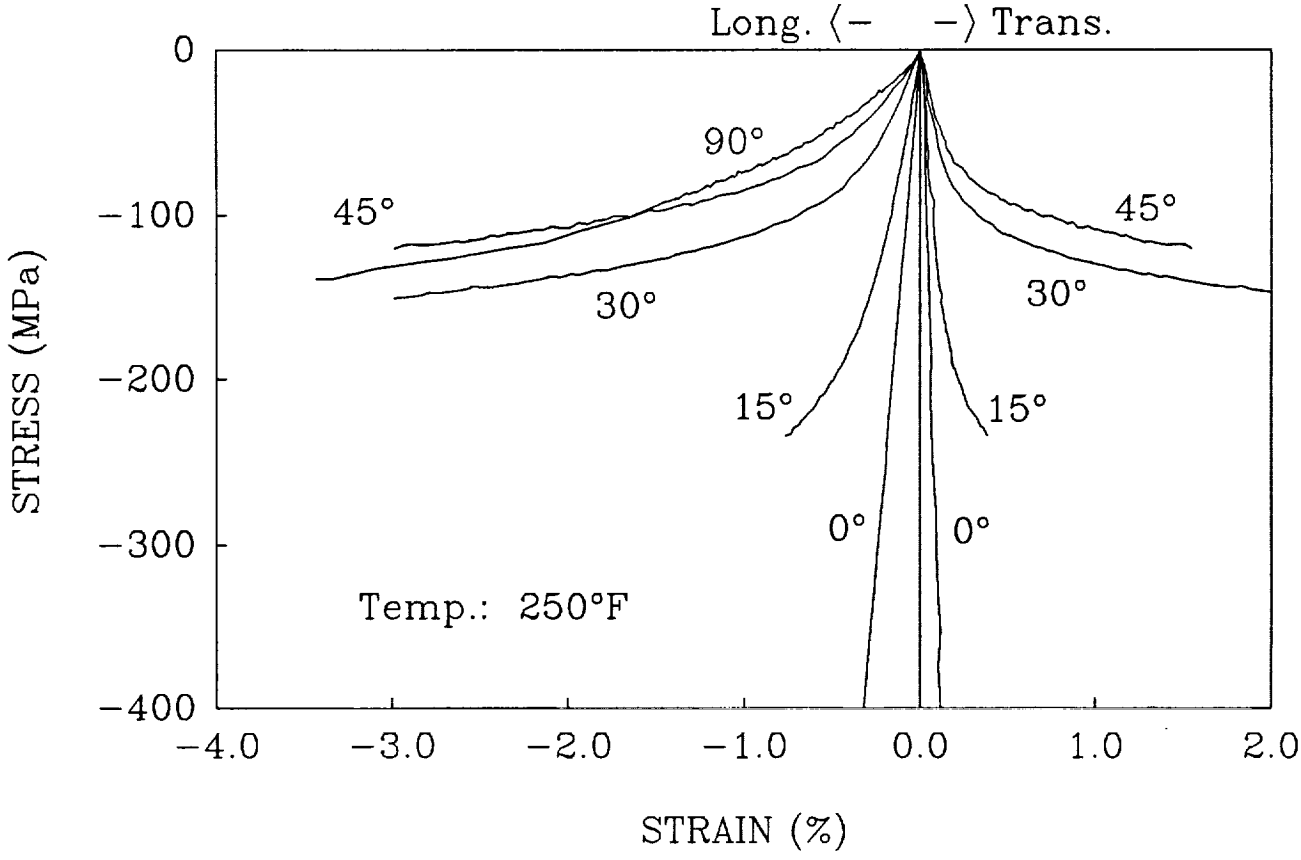

Fig. 4. Compressive stress-strain curves for off-axis specimens of AS4/APC-2 at 250°F.

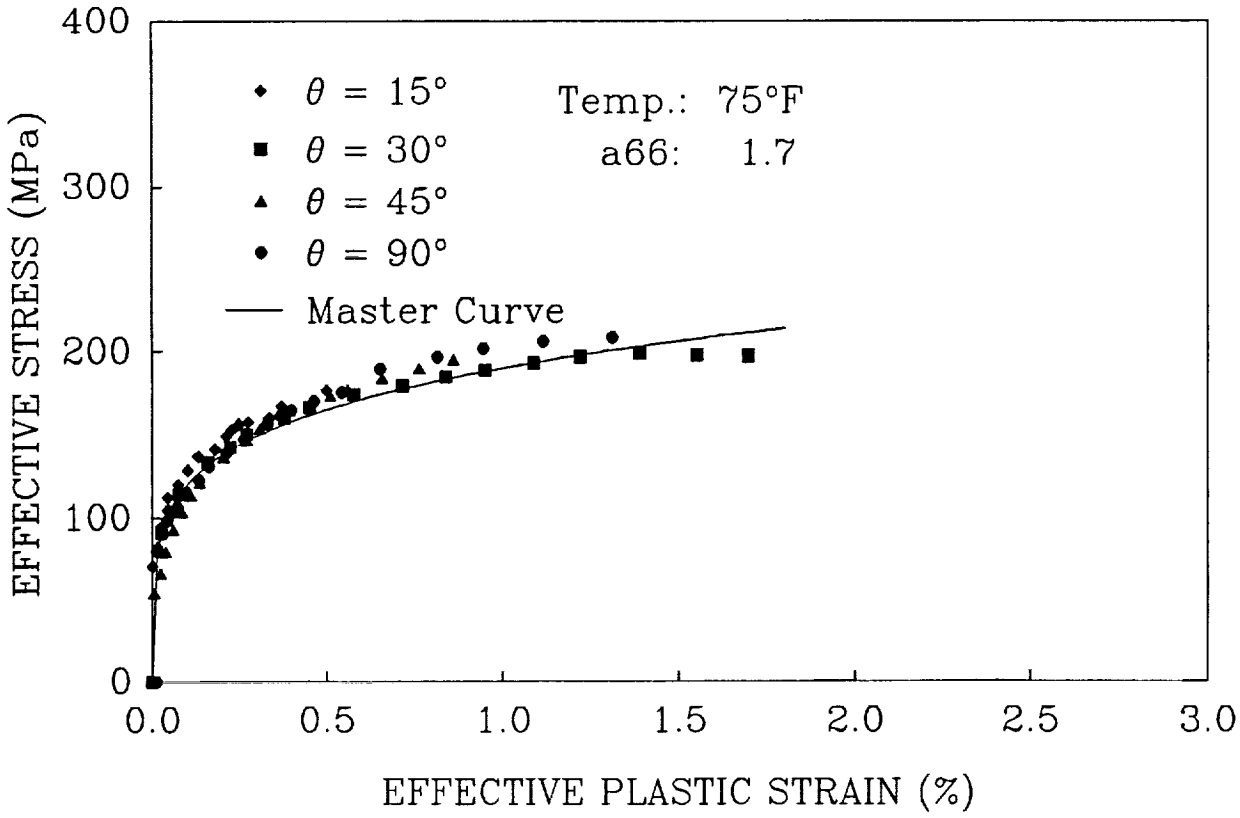

Fig. 5. Effective stress-effective plastic strain curves for off-axis specimens of AS4/APC-2 with $a_{66} = 1.7$ at 75°F.

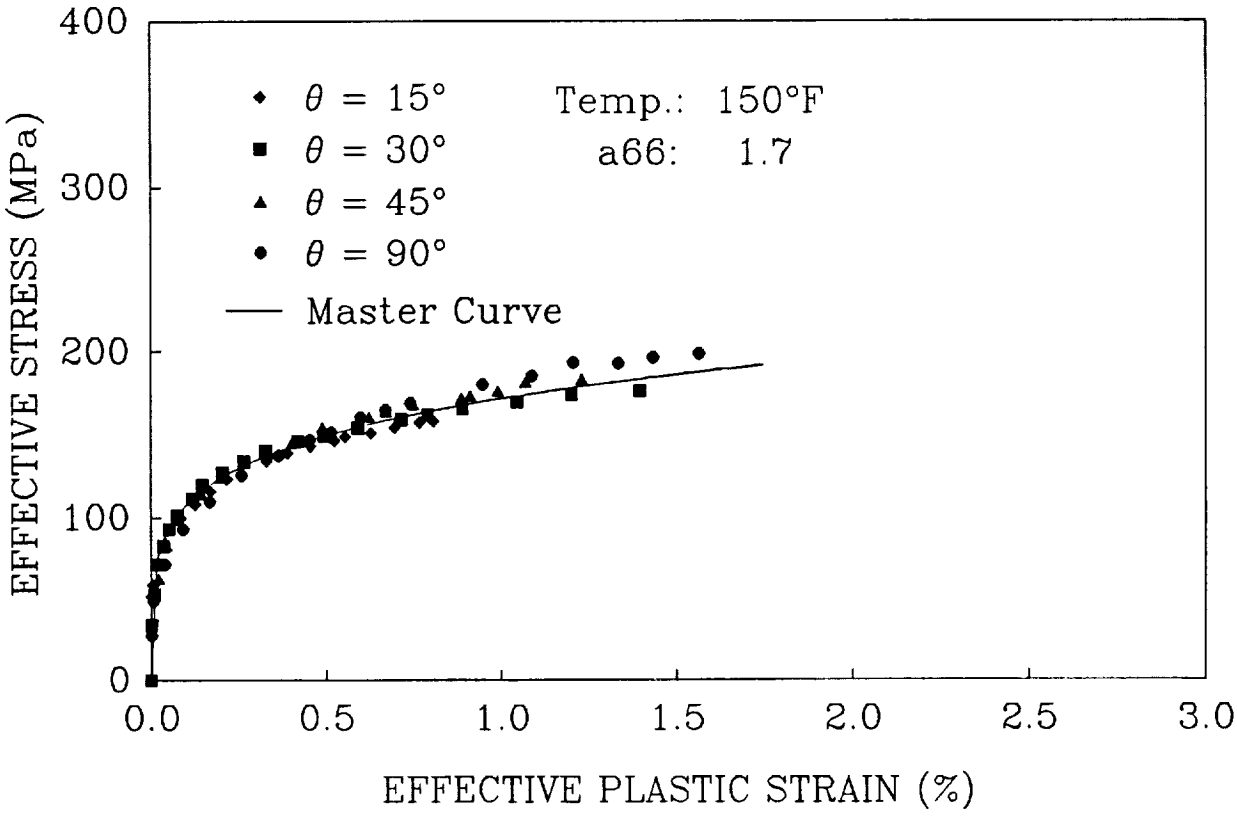

Fig. 6. Effective stress-effective plastic strain curves for off-axis specimens of AS4/APC-2 with $a_{66} = 1.7$ at 150°F.

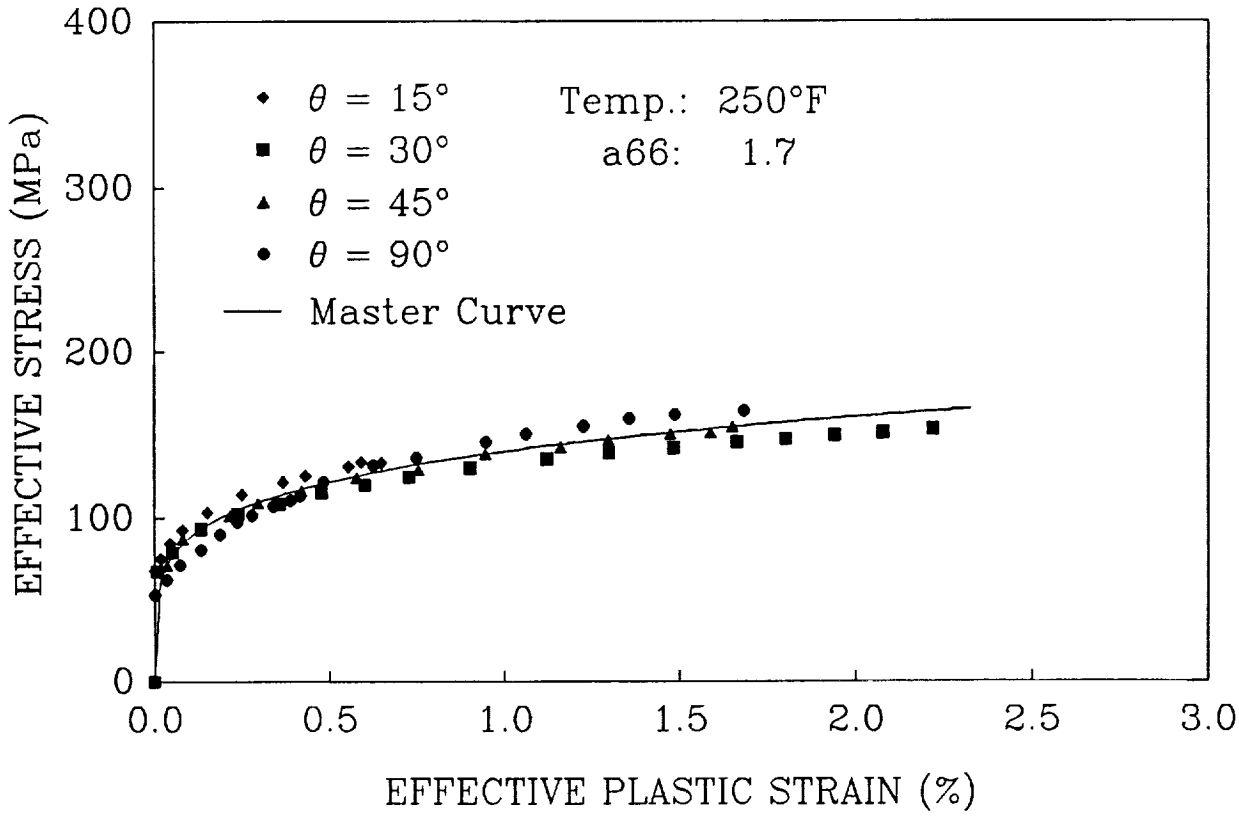

Fig. 7. Effective stress-effective plastic strain curves for off-axis specimens of AS4/APC-2 with $a_{66} = 1.7$ at 250°F.

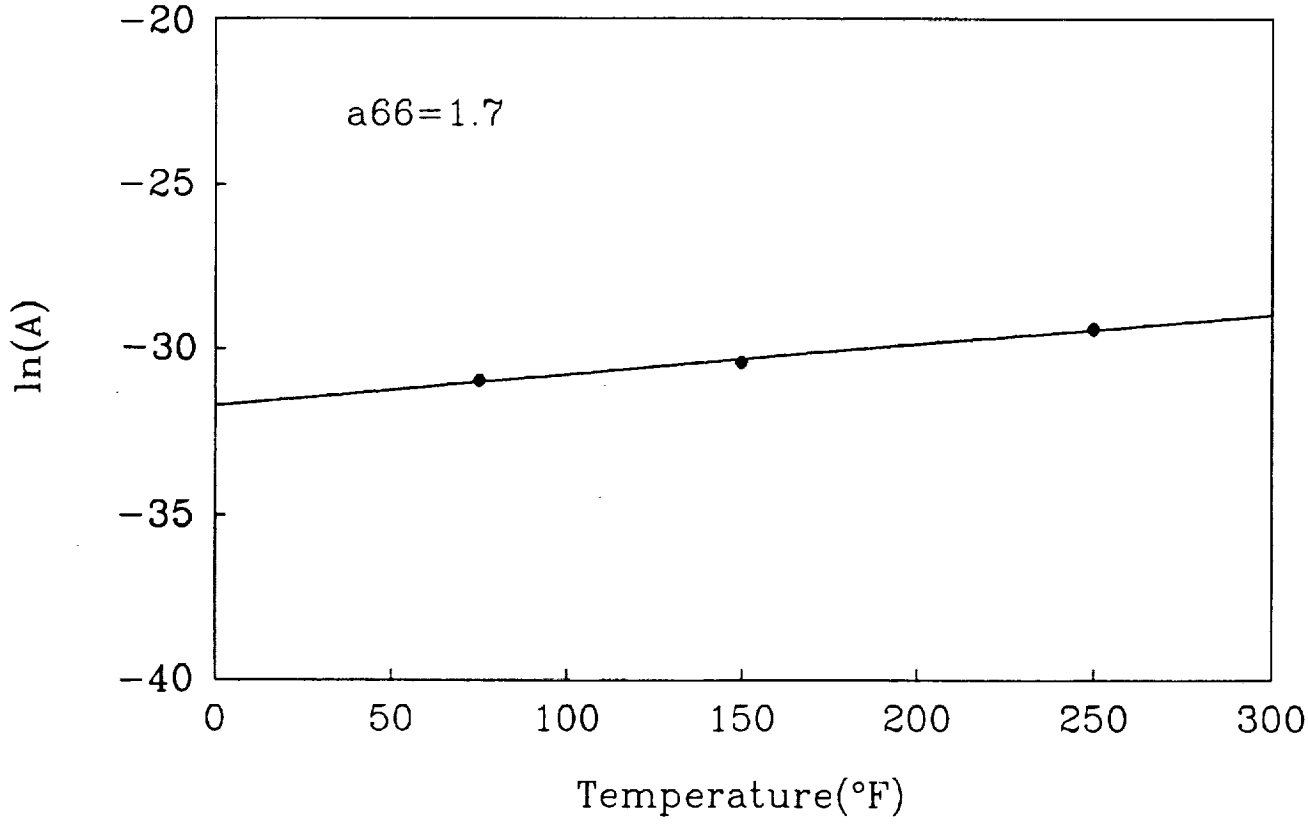

Fig. 8. Variation of ln(A) with temperature (unit of A: MPa^{-5}).

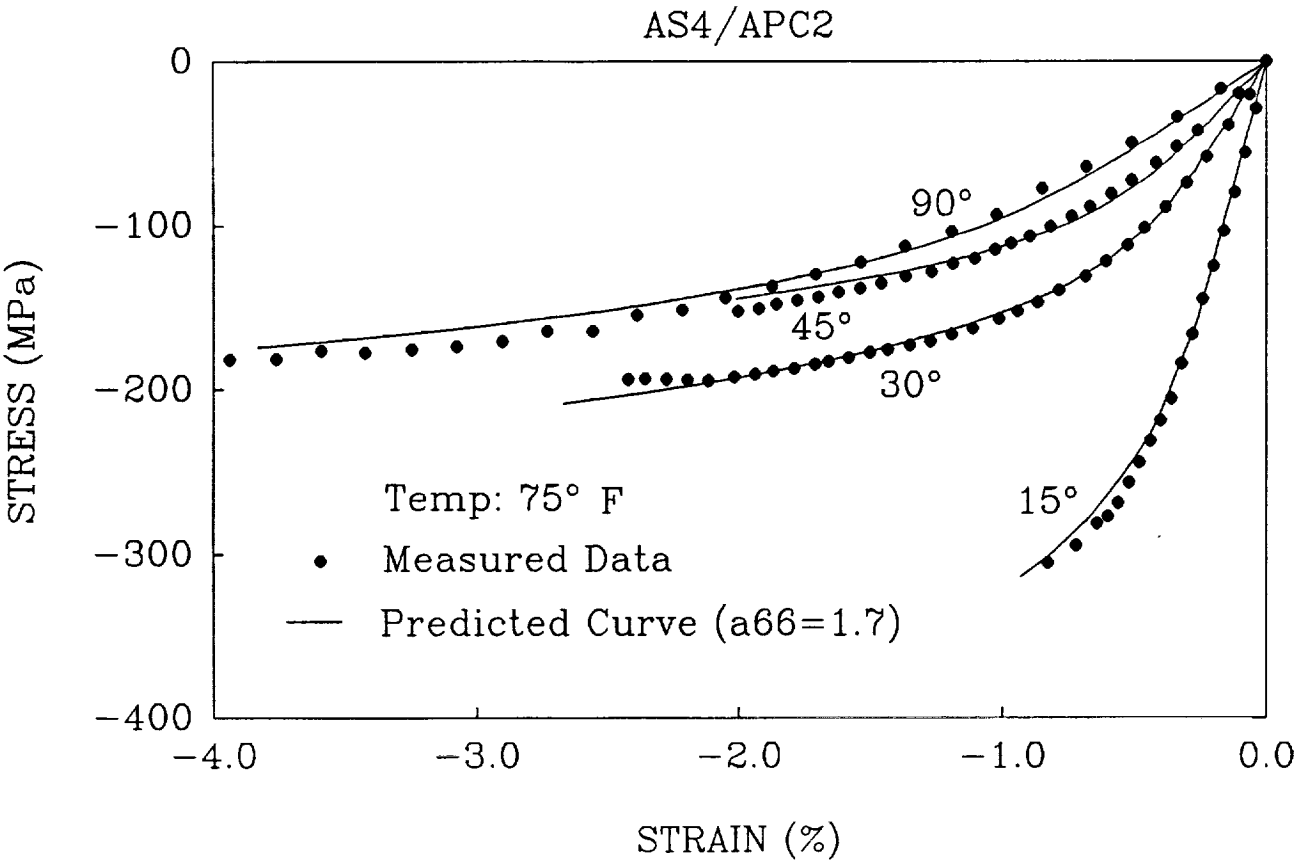

Fig. 9. Comparison of compressive stress-strain curves for off-axis specimens of AS4/APC-2 obtained from experiment and from the one-parameter plasticity model at 75°F.

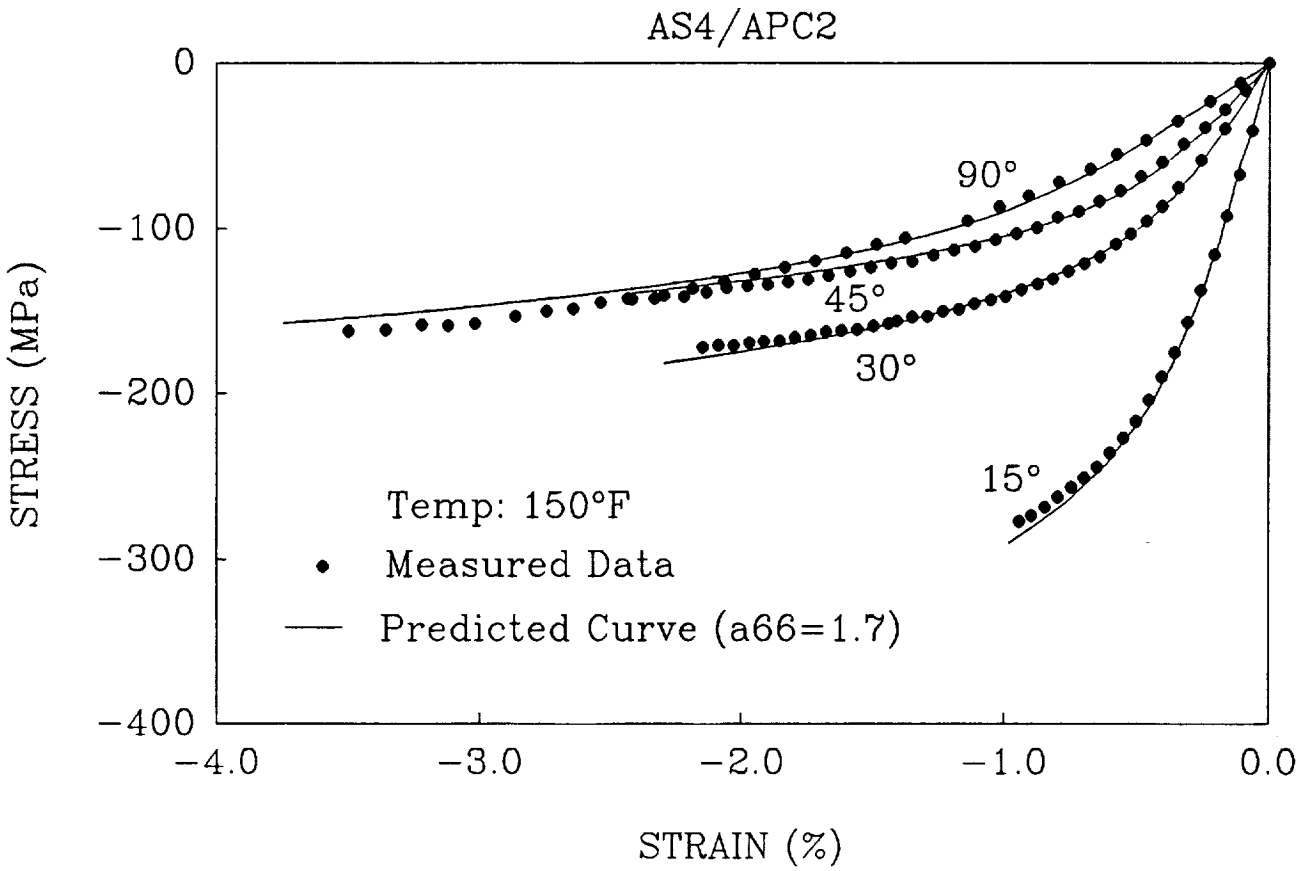

Fig. 10. Comparison of compressive stress-strain curves for off-axis specimens of AS4/APC-2 obtained from experiment and from the one-parameter plasticity model at 150°F.

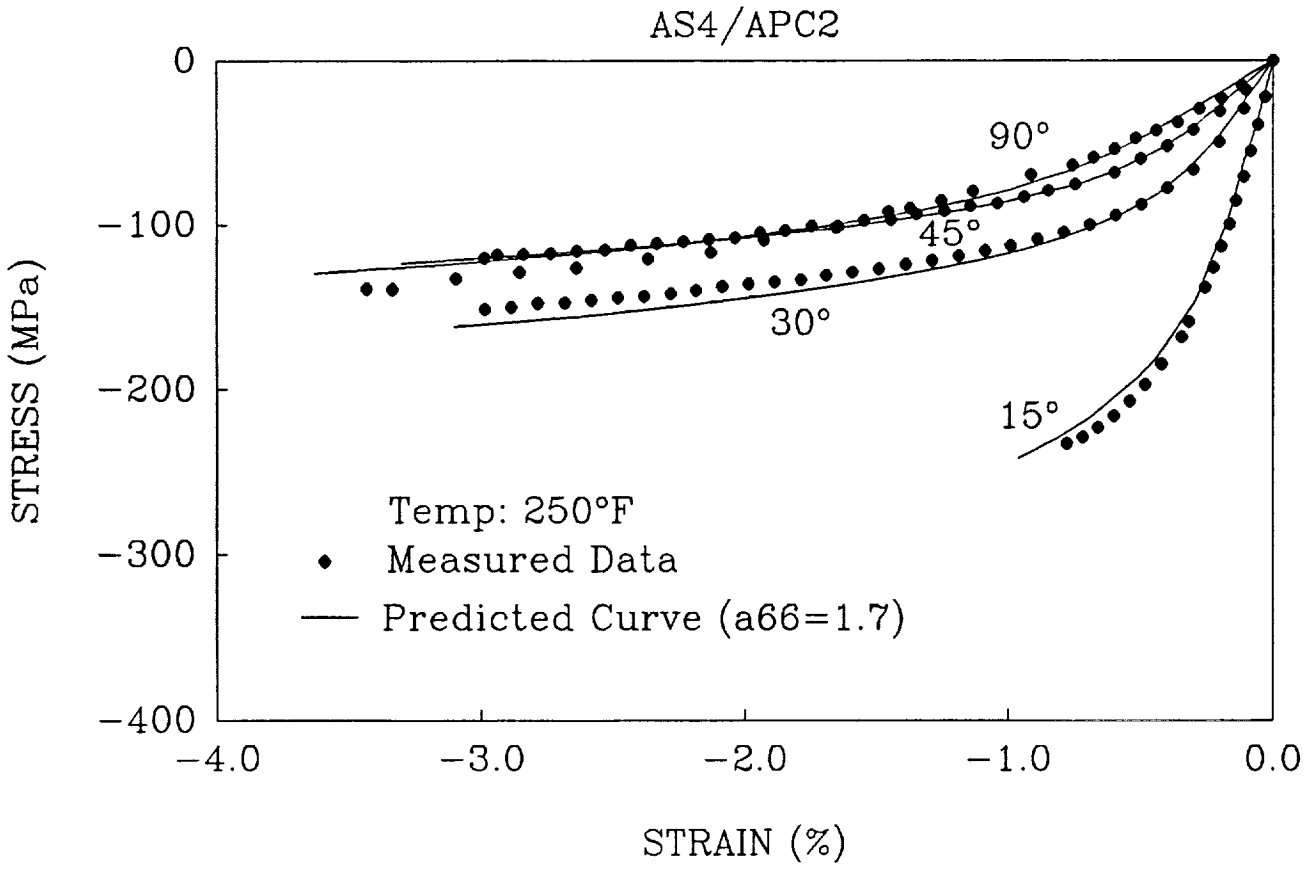

Fig. 11. Comparison of compressive stress-strain curves for off-axis specimens of AS4/APC-2 obtained from experiment and from the one-parameter plasticity model at 250°F.

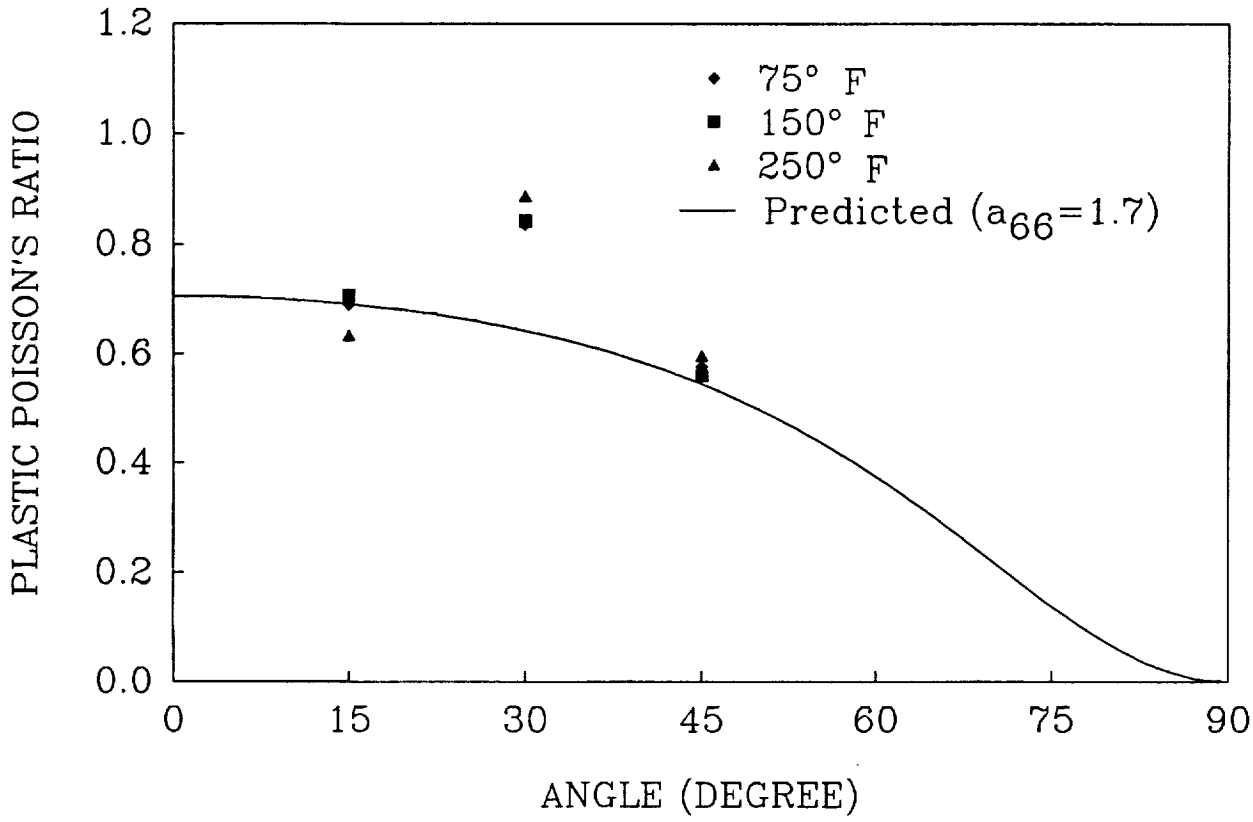

Fig. 12. Plastic Poisson's ratios of AS4/APC-2 obtained from experiment and from the one-parameter plasticity model with $a_{66} = 1.7$.

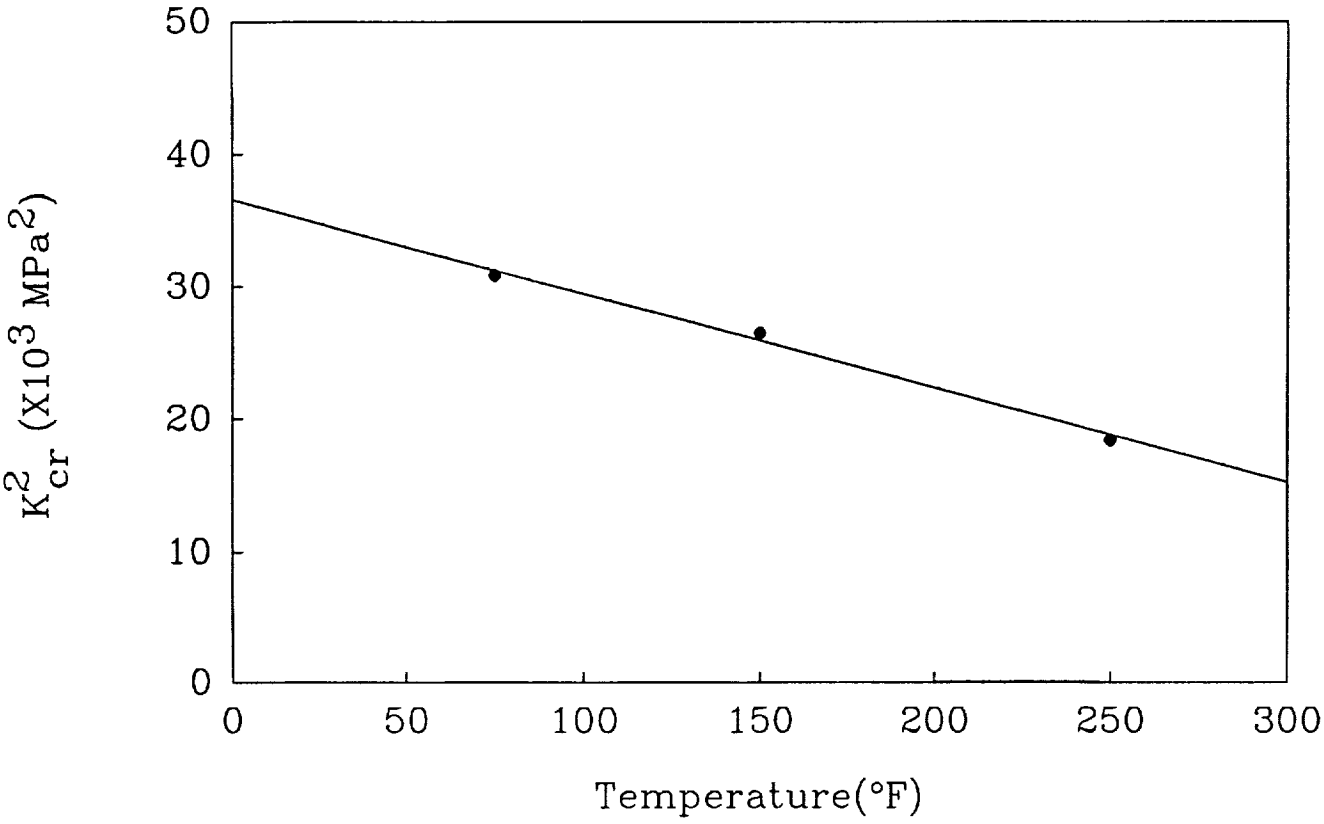

Fig. 13. Variation of k^2_{cr} with temperature.

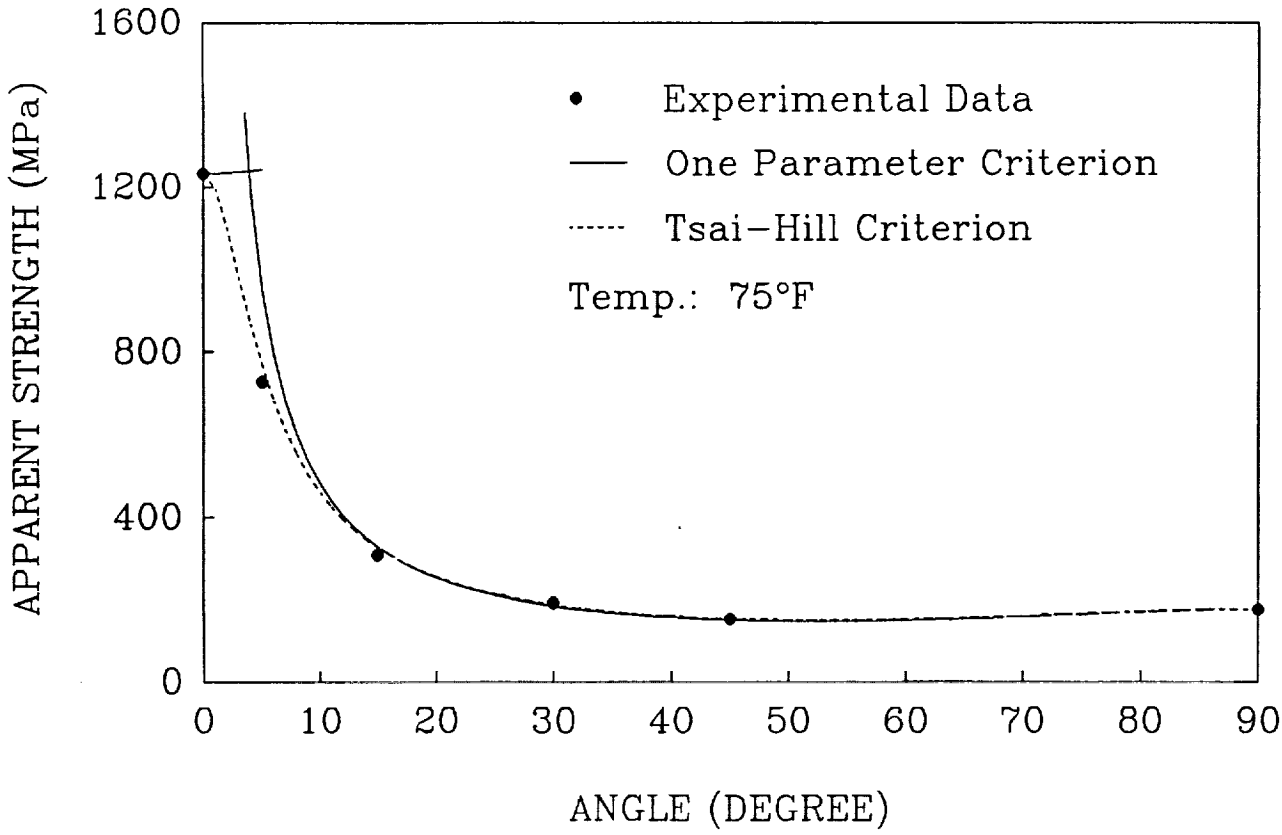

Fig. 14. Comparison of compressive strengths for off-axis specimens of AS4/APC-2 obtained from experiment, Tsai-Hill criterion and one-parameter criterion at 75°F.

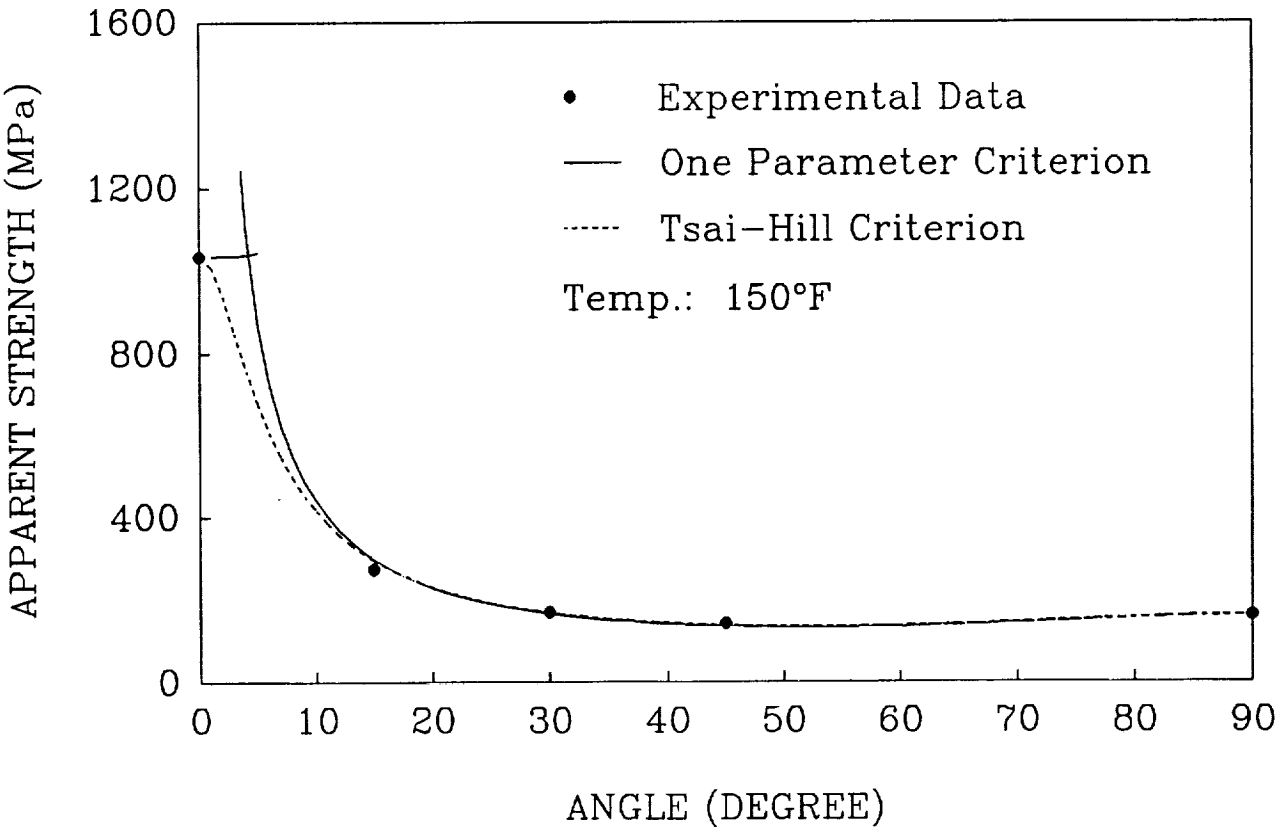

Fig. 15. Comparison of compressive strengths for off-axis specimens of AS4/APC-2 obtained from experiment, Tsai-Hill criterion and one-parameter criterion at 150°F.

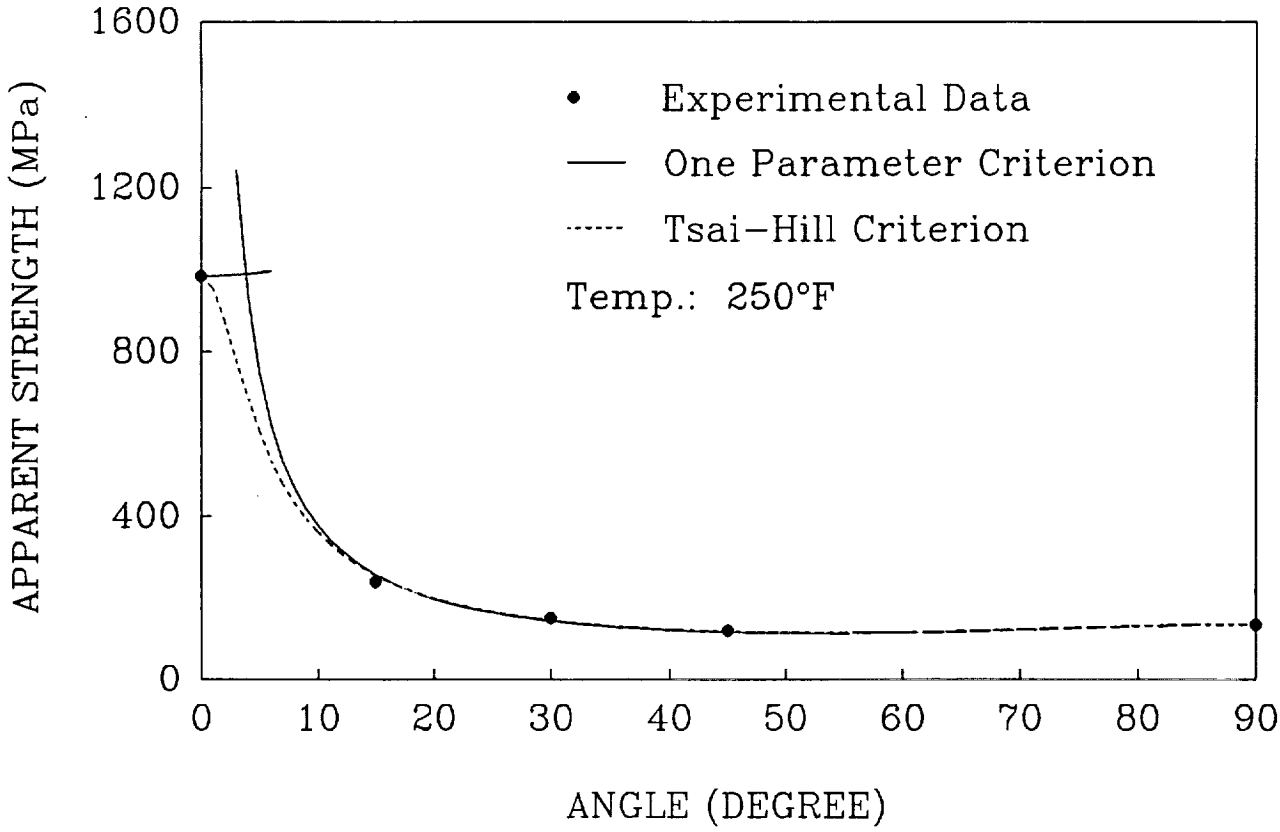

Fig. 16. Comparison of compressive strengths for off-axis specimens of AS4/APC-2 obtained from experiment, Tsai-Hill criterion and one-parameter criterion at 250°F.